

**Linn, J., Kloker, M.J. 2007**  
**Numerical investigations of effusion cooling in hypersonic boundary-layer flow. In: *New Results in Numerical and Experimental Fluid Dynamics VI* (ed. S. Jakirlic, C. Tropea, H.-J. Heinemann, R. Hilbig), NNFM series, Springer.**

# Numerical Investigations of Effusion Cooling in Hypersonic Boundary-Layer Flow

Jens Linn and Markus J. Kloker

Institut für Aerodynamik und Gasdynamik, Universität Stuttgart,  
Pfaffenwaldring 21, D-70550 Stuttgart, Germany  
<lastname>@iag.uni-stuttgart.de

## Summary

Direct numerical simulations (DNS) are carried out to investigate the effect of effusion cooling by blowing through spanwise slits and discrete holes in a laminar flat-plate boundary layer at various Mach numbers. The comparison with experimental data for a Mach-2.67 boundary layer with a cool wall and a spanwise slit shows good agreement. For an adiabatic Mach-6 boundary layer, the focus of the study is the effectiveness of various effusion-cooling configurations (slits and holes), the generated vortices and shear-layer systems. In terms of cooling effectiveness slits are preferable over (a few) holes.

## 1 Introduction

For aerospace or hypersonic cruise vehicles, the state of the boundary layer is of great importance, because for turbulent boundary layers, the thermal loads and skin friction are higher than in laminar boundary layers. Therefore, knowledge of cooling features and laminar-turbulent transition is necessary for the design and the thermal protection system (TPS). Different strategies are used to reduce the thermal loads of hypervelocity vehicles, e.g. radiation, transpiration, effusion cooling or ablation. The subject of this paper is the effusion or film cooling, where cold air is blown into the boundary layer through spanwise slits or rows of holes. This implies a change in the laminar stability properties of the boundary layer.

## 2 Numerical Method and Boundary Conditions

The numerical method is based on the complete 3-d unsteady compressible Navier-Stokes equations in conservative formulation ( $\rho$ ,  $\rho u$ ,  $\rho v$ ,  $\rho w$  and  $\rho e$ ). The equations are solved in a rectangular integration domain on the flat plate, which does not contain any shock wave induced by the leading edge. In streamwise ( $x$ -) and wall-normal ( $y$ -) direction, the discretisation is realized by splitted compact finite differences of 6<sup>th</sup> order [7]. In the spanwise ( $z$ -) direction, the flow is assumed to be periodic, thus a Fourier spectral representation is employed. The time integration is done with a classical 4<sup>th</sup>-order Runge-Kutta method. A detailed description of the

discretisation and the algorithm is reported in [1].

All length scales are nondimensionalised with respect to a reference length  $L^* = \frac{\nu_\infty^* Re}{u_\infty^*}$ . Reference values for velocity, density, temperature, viscosity and conductivity are their freestream values at the inflow (indicated by subscript  $\infty$ ). The pressure is normalised by  $\rho_\infty^* u_\infty^{*2}$ , where the superscript  $\star$  denotes the dimensional quantities. With these definitions, the global Reynolds number is defined as  $Re = \frac{u_\infty^* L^*}{\nu_\infty^*} = 10^5$ . The air is considered as a non-reacting calorically perfect gas [3, 9].

At the inflow boundary ( $x = x_0$ ), profiles from boundary-layer theory are fixed for all flow variables. For the boundary conditions at the outflow ( $x = x_N$ ), all equations are solved neglecting the second  $x$ -derivative terms. At the freestream boundary ( $y = y_M$ ), the gradient of the flow variables is set to zero along spatial characteristics [3].

The steady blowing of cold air through holes at the wall with a radius  $r_c$  (figure 1) is modelled by prescribing a wall-normal momentum distribution

$$(\rho v) = (\rho v)_{c,max} \cdot c(r) \quad , \quad (1)$$

where  $(\rho v)_{c,max}$  is the maximum wall-normal momentum (maximum blowing ratio). The wall temperature distribution over the hole is prescribed by

$$T_c = T_w \cdot (1 - c(r)) + T_{c,core} \cdot c(r) \quad , \quad (2)$$

where  $T_{c,core}$  is the core temperature of the cold air and  $T_w$  the local wall temperature at the edge of the hole. The distribution function  $c(r)$  is a polynomial of 5<sup>th</sup> order, which has been already used in [10] for suction and blowing to generate disturbances at the wall. Both the gradient and curvature are zero at  $r = 0$  and  $r = r_c$ :

$$c(r) = 1 - 6 \cdot \left(\frac{r}{r_c}\right)^5 + 15 \cdot \left(\frac{r}{r_c}\right)^4 - 10 \cdot \left(\frac{r}{r_c}\right)^3 \quad , \quad (3)$$

$$r = \sqrt{(x - x_c)^2 + (z - z_c)^2} \quad , \quad 0 \leq r \leq r_c \quad ,$$

where  $x_c$  and  $z_c$  stand for the center coordinates of the hole. Outside the hole,  $(\rho v)$  is zero at the wall,  $T_w$  is the local adiabatic wall temperature ( $(\partial T / \partial y)|_w = 0$ ) or has a constant value (isothermal wall), and the pressure gradient in wall-normal direction at the wall and in the holes is zero. For steady blowing through a spanwise slit of width  $b_c = 2 \cdot r_c$ , the distribution function  $c(r)$  in equation (3) is independent from the  $z$ -coordinate, i.e.  $z = z_c$ .

Grid refinements studies showed no dependence of the grid spacing ( $\Delta x$ ,  $\Delta y$ ,  $\Delta z$ ,  $\Delta t$ ) on the steady state solutions discussed below.

### 3 Results

#### 3.1 Comparison with Experiments at Mach 2.67

In this section, we compare our simulation results with the measurements of Heufer and Olivier [4, 5] at the Shock Wave Laboratory Aachen (SWL). They investigated

an isothermal laminar boundary layer on a wedge with a deflection angle of  $30^\circ$  and a given post-shock Mach number 2.67, with  $M = 7$  and  $T_0^* = 1368K$ . Cold air is blown through one spanwise slit. The given post-shock freestream temperature is  $T_\infty^* = 564K (\approx 0.45 T_{rec}^*)$ , the pressure  $p_\infty^* = 0.1489bar (\Rightarrow L^* = 24.57mm)$ , and the wall temperature is  $T_W^* = 293K = const (\approx \frac{1}{4} T_{rec}^*)$ . This wall temperature means that the wall is strongly cooled. Investigations based on the Linear Stability Theory (LST) have shown (see, e.g.[8]), that wall cooling stabilises 1<sup>st</sup>-mode (vorticity) disturbances and destabilises the 2<sup>nd</sup>-mode (acoustic) disturbances that do not exist at Mach numbers lower than approximately 3.5. In addition, the basic boundary layer investigated is subcritical ( $R_{x,crit} \gg Re_x(x_N)$ ) due to the strong wall cooling.

Figure 2 shows the comparison of the experimental [4, 5] and the simulation data for two blowing ratios,  $(\rho v)_{c,max} = 0.043$  and  $(\rho v)_{c,max} = 0.065$ , with  $T_{c,core}^* = 293K (= T_w^*)$ . The slit width is  $b_c^* = 0.5mm (\approx 0.57 \delta_c)$ ,  $\delta_c$  - boundary-layer thickness), and the cooling effectiveness is defined by  $\eta_c = 1 - \dot{q}_c/\dot{q}_{ref}$ , where  $\dot{q}_c = \vartheta \cdot \partial T/\partial y|_w$  is the heat flux into the wall with effusion cooling and  $\dot{q}_{ref}$  is the heat flux without effusion cooling. For both blowing rates the cooling effectiveness is higher in the simulations. In the low-blowing case, there is a heat flux into the slit and cold-gas reservoir in the experiment resulting in a higher cooling gas temperature  $T_{c,core}^*$  (that was realized but not quantitatively measured) thus lowering the cooling effectiveness  $\eta_c$ . Note that no experimental data of the boundary-layer evolution are available and thus the local thickness parameters and Reynolds numbers may differ. Higher cooling effectiveness was also found by tentative numerical simulations at SWL. A longitudinal cut of the temperature field with streamlines is shown in figure 3 for the high blowing rate. In front of the slit is a reversed-flow region near the wall with a clockwise rotating vortex with its center marked by the dot.

For both blowing rates, no instability regions were found using LST despite a separation region exists in front of the slit. The basic cooling by the cool wall is so strong that it stabilizes even the blowing. Here effusion cooling is applied in a case where the flow is already strongly cooled by a cool wall, thus this case is unrealistic. A simple transfer of the results to cases with significantly different wall temperature gradients is not possible.

### 3.2 Comparison of Effusion-Cooling Configurations at Mach 6

In this section we investigate an adiabatic boundary layer at an edge Mach number 6 in which cold air is blown through spanwise slits and rows of holes. The freestream temperature is  $T_\infty^* = 89K (\approx \frac{1}{7} T_{rec}^*)$  and the pressure is  $p_\infty^* = 0.0038bar (\Rightarrow L^* = 36.28mm)$ , matching the flow parameters of experiments in the hypersonic wind tunnel H2K of DLR-Köln [2]. Table 1 summarizes the parameters. Slits were used in cases *a*, *b* and holes in cases *c*, *d*. The integrally injected massflow and the cooling gas temperature  $T_{c,core}^* = 293K (\approx \frac{1}{2} T_{rec}^*)$  is in all cases the same. In case *c* the two rows of holes are aligned in contrast to case *d* where the rows are  $s_z/2$ -staggered. The first spanwise slit or row of holes is positioned at  $x_c = 2.205$ .

The resulting wall temperature is shown in figure 4 for all four configurations. Cases *a* and *b* look very similar and show a significant lower wall temperature than the two other cases *c* and *d*. In the „aligned” case *c*, the wall temperature is only slightly reduced and strongly varies in the  $z$ -direction. In the „staggered” case *d*, the wall temperature is lower than in case *c*, and does not vary as strong in the  $z$ -direction. The temperature and  $u$ -distribution in the crosscut is shown in figure 5. The aligned rows blow more cold gas from the wall into the boundary layer and show stronger  $\frac{\partial u}{\partial z}$ -gradients than the staggered rows. The reason why the slits are more efficient is that the blowing surface is much larger than with the holes, translating into a lower wall-normal velocity in the slits. Thereby the cold gas keeps closer to the wall. The vortical structures of the hole configurations are visualised via the  $\lambda_2$ -criterion [6] in figure 6. From the holes, counter-rotating vortex pairs (CVPs) emerge which are along the jet trajectory and have such a rotation sense that gas is transported away from the wall in the streamwise hole center line. Furthermore exists a toroidal neck vortex at each hole edge. It has a counter-clockwise rotation sense upstream the hole, in contrast to the considered slit case. A horseshoe vortex is not observed in the simulations due to the low blowing ratio. In studies of jets in crossflow (JICF), where typically a horseshoe vortex (with a rotation sense opposite to the CVP) is found,  $(\rho v)_{c,max} \approx \mathcal{O}(1)$  and  $d > \delta$ . In the aligned case (figure 6a), the second row enhances the CVPs from the first row and the vortices lay wall-parallel. In contrast, figure 6b shows the CVPs from the second row pushed downwards, keeping the cold gas at the wall. However, the CVPs of both cases decay downstream. For a Mach-6 boundary layer, the strongest amplified disturbance mode is the  $2^{nd}$  mode as a 2-d wave ( $\gamma = 0$ ). Figure 7 shows the stability diagram for case *a*. The dash-dotted lines mark the streamwise positions of the slit centers. The  $1^{st}$  mode is completely stabilised for  $\gamma = 0$  because of the cooled wall and is not present anymore in the considered streamwise region. The  $2^{nd}$  mode is shifted to lower frequencies in the region of the slits, and the maximum amplification rate  $\alpha_{i,max}$  is about twice as large as in the case without blowing. A small additional instability region is developed at the slits over the  $2^{nd}$  mode, which seems a higher viscous mode. Figure 8 shows the N-factors for case *a* with and without blowing. For the frequency  $\omega = 12.5$  the N-factor is approximately four times higher at the end of the considered streamwise domain than without blowing. Primary LST uses the assumption that the spanwise base-flow gradients are zero. This assumption is no longer valid in the cases *c* and *d* with the holes and therefore primary LST can not be used to predict the instability of these cases. For cases *c* and *d*, unsteady background disturbances will be introduced in the DNS to investigate the instability properties of the full 3-d case. Enhanced laminar instability can compromise the cooling effect.

## 4 Conclusions

The comparison between numerical and experimental results for effusion cooling of a laminar, basically already cooled isothermal Mach-2.67 boundary layer through

slits shows good agreement. The simulation predicts a slightly higher cooling effectiveness which may be caused by differing boundary-layer parameters that are not available from the experiment.

The presented results for effusion-cooling configurations with slits and holes of an adiabatic Mach-6 boundary layer shows that slits are better than (a few) holes. The slit blowing velocity is, at same mass flow, smaller than that of (a few) holes. Aligned rows of holes induce a strong variation of the wall temperature and less cooling effectiveness compared to staggered rows of holes. A counter-rotating vortex pair (CVP) is generated at each hole, decaying downstream. In the staggered case, the decay is stronger than in the aligned case. The analysis with the linear stability theory shows that the maximum amplification rate of  $2^{nd}$ -mode disturbances grows and the amplified frequency band is shifted to lower frequencies. Defined 3-d instability investigations will be performed by unsteady DNS.

## Acknowledgments

This research has been partially sponsored by the Helmholtz-Gemeinschaft (HGF) within the German joint project RESPACE - Key Technologies for Reusable Space Systems.

## References

- [1] Babucke, A., Linn, J., Kloker M., Rist, U.: "Direct numerical simulation of shear flow phenomena on parallel vector computers", In *High Performance Computing on Vector Systems* (ed. M. Resch & el.) Proc. High Performance Computing Center Stuttgart, pp. 229-247, Springer (2006).
- [2] Bierbach, M.: "Untersuchungen zur aktiven Kühlung der Grenzschichtströmung an einem Plattenmodell", Diplomarbeit, Technische Universität Darmstadt (2005).
- [3] Eißer, W.: "Numerische Untersuchungen zum laminar-turbulent Strömungsumschlag in Überschallgrenzschichten", Dissertation, Universität Stuttgart (1998).
- [4] Heufer, K.A., Olivier, H.: "Film cooling for hypersonic flow conditions", *Proc. 5th European Workshop on Thermal Protection Systems and Hot Structures 2006*, ESA.
- [5] Heufer, K.A., Olivier, H.: "Film Cooling of an Inclined Flat Plate in Hypersonic Flow", AIAA 2006-8067.
- [6] Jeong, J., Hussain, F.: "On the identification of a vortex", *J. Fluid Mech.*, vol. 285, pp. 69-94 (1995).
- [7] Kloker, M.: "A robust high-resolution split-type compact FD-scheme for spatial direct numerical simulation of boundary-layer transition", *Applied Scientific Research*, vol. 59, pp. 353-377 (1998).
- [8] Malik, M.R.: "Prediction and control of transition in supersonic and hypersonic boundary layers", *AIAA-J.*, vol. 27, pp. 1487-1493 (1989).
- [9] Thumm, A.: "Numerische Untersuchung zum laminar-turbulenten Strömungsumschlag in transsonischen Grenzschichtströmungen", Dissertation, Universität Stuttgart (1991).
- [10] Stemmer C., Kloker M.: "Interference of wave trains with varying phase relations in a decelerated 2-d boundary layer", In *Recent Results in Laminar-Turbulent Transition* (ed. S. Wagner, M. Kloker, U. Rist), *NNFM*, vol. 86, pp. 91-110, Springer (2003).

**Table 1** Parameters of the slits and holes configurations for cases at  $M_e = 6$

case	slits	row of holes	$(\rho v)_{c,max}$	hole diameter or slit width $d$	streamwise spacing $s_x$	spanwise spacing $s_z$	rows z-offset
a	2	-	0.0284	$0.058 \approx 0.6 \delta$	$0.1378 \approx 1.4 \delta$	-	-
b	1	-	0.0284	0.087	0.1378	-	-
c	-	2	0.15	0.058	0.1378	0.1378	-
d	-	2	0.15	0.058	0.1378	0.1378	$s_z/2$

$x_0 = 0.225, \quad x_N = 7.33, \quad y_M = 0.54 \approx 4 \delta \text{ at } x = x_N,$   
 $Pr = 0.71, \quad \kappa = 1.4, \quad \mu^*(T) = \mu^*(T_\infty) \cdot T^{3/2} \cdot \frac{1+T_S}{T+T_S}$   
 with  $S = \frac{110.4}{T^*}$  and  $\mu_\infty^*(T_\infty = 280K) = 1.735 \cdot 10^{-5} \frac{kg}{ms}$

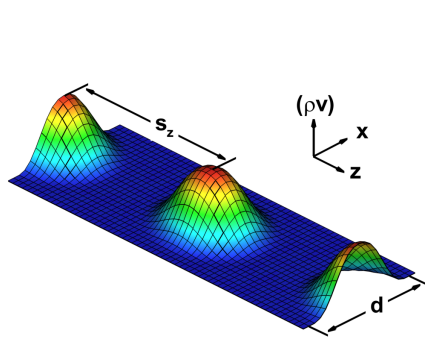


**Figure 1**  $(\rho v)$ -distribution at the wall for one row of holes

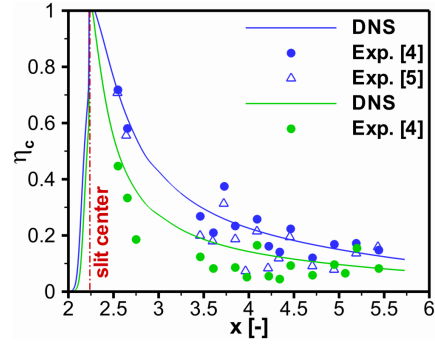


**Figure 2** Comparison of cooling effectiveness  $\eta_c$  from simulation and experiment for an effusion cooled boundary layer at Mach 2.67 for two blowing rates ( blue -  $(\rho v)_{c,max} = 0.065$ ; green -  $(\rho v)_{c,max} = 0.043$ ).

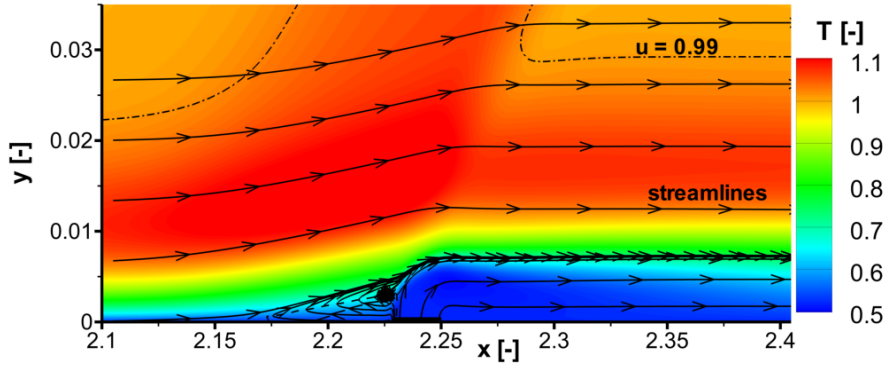


**Figure 3** Visualisation of the temperature field with streamlines in a longitudinal cut for the effusion-cooled boundary layer at Mach 2.67 ( $(\rho v)_{c,max} = 0.065$ ). Isolines of the  $u$ -velocity for  $u = 0$  (dashed line) and  $u = 0.99$  (dashed dotted line).  $\Delta x = 0.253 \cdot 10^{-2}$  and  $\Delta y = 0.6 \cdot 10^{-3}$ .

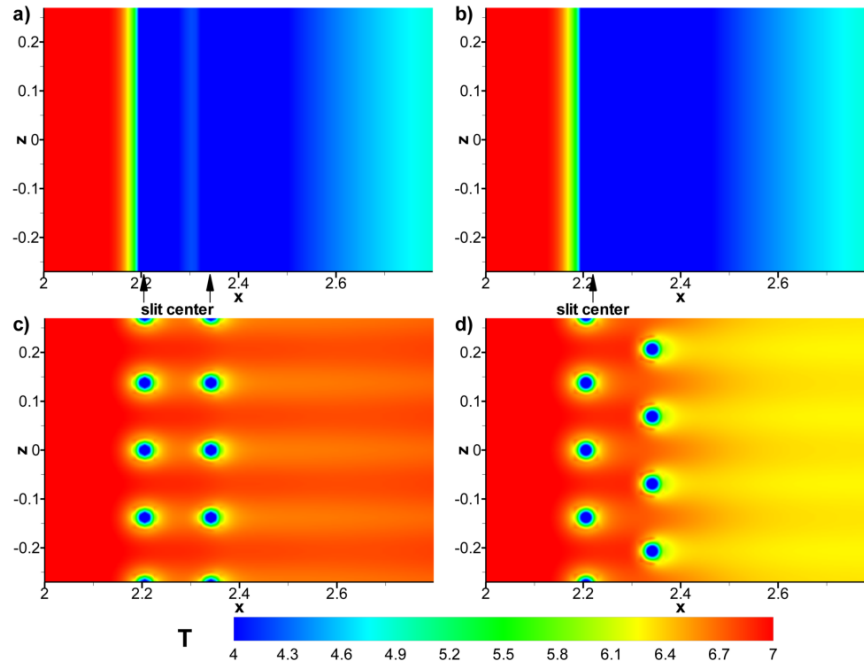


**Figure 4** Wall temperature for steady blowing into an adiabatic flat-plate boundary layer at Mach 6 through two spanwise slits (a), one slit (b), two aligned rows of holes (c) and two  $s_z/2$ -staggered rows of holes (d).

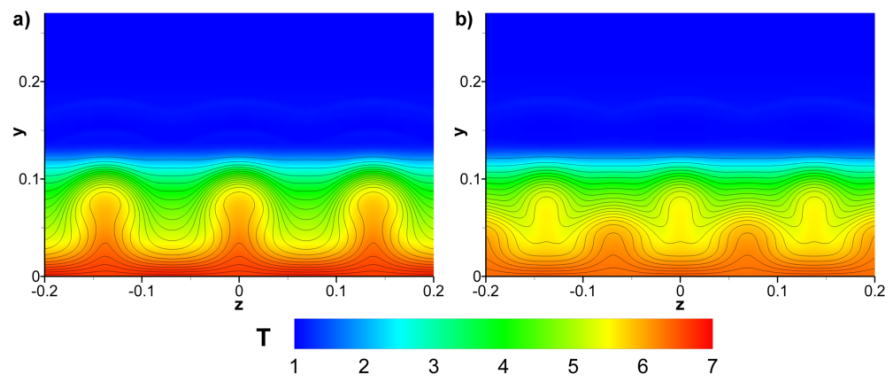


**Figure 5** Visualisation of the temperature field and isolines of the  $u$ -velocity in the crosscut at  $x = 2.5$  for the aligned rows (a) and for the  $s_z/2$ -staggered rows (b).

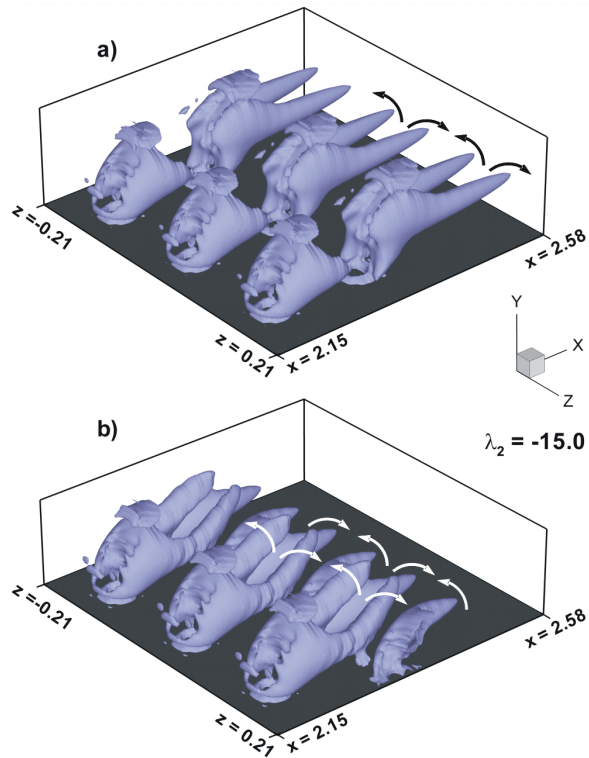


**Figure 6** Visualisation of vortical structures via  $\lambda_2$ -isosurface ( $\lambda_2 = -15.0$ ) for aligned rows of holes (a) and for staggered rows of holes (b). The arrows indicate the rotation sense.

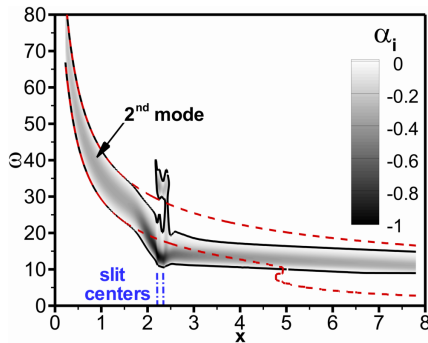


**Figure 7** Stability diagram (from LST) for an adiabatic, effusion-cooled Mach-6 boundary layer (case *a*) for a ( $2^{\text{nd}}$ -mode) 2-d wave (frequency:  $\omega = \frac{2\pi L^* f^*}{u_\infty^*}$ ). Dashed red line is the  $\alpha_i = 0$  curve of the adiabatic Mach-6 boundary layer without blowing, displaying also  $1^{\text{st}}$ -mode instability for  $x > 4.7$ .

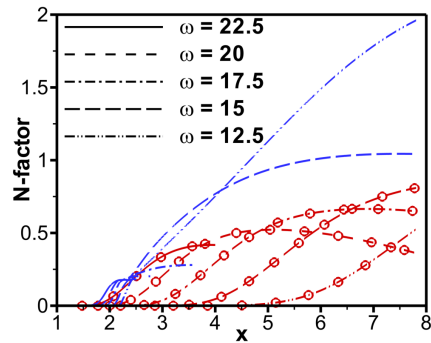


**Figure 8** N-factors ( $= -\int_{x_0}^x \alpha_i dx$ ) of case *a* with (blue lines) and without blowing (red lines with circles) for various frequencies  $\omega$  (see also figure 7).